

Implementation of an all-electron GW approximation based on the PAW method without plasmon pole approximation: application to Si, SiC, AlAs, InAs, NaH and KH

S. Lebègue,^{1,2} B. Arnaud,³ M. Alouani,^{1,4} and P. E. Bloechl^{4,5}

¹*Institut de Physique et de Chimie des Matériaux de Strasbourg (IPCMS),
UMR 7504 du CNRS, 23 rue du Loess, 67037 Strasbourg, France, EU*

²*Department of Physics, University of California, Davis, California 95616*

³*Groupe Matière condensée et Matériaux (GMCM),*

Campus de Beaulieu - Bat 11A 35042 Rennes cedex, France, EU

⁴*Kavli Institute of Theoretical Physics, University of California, Santa Barbara, Ca 93111*

⁵*Institute of Theoretical Physics, Clausthal University of Technology,
Leibnizstr. 10 D-38678 Clausthal Zellerfeld, Germany, EU*

(Dated: June 5, 2018)

A new implementation of the GW approximation (GWA) based on the all-electron Projector-Augmented-Wave method (PAW) is presented, where the screened Coulomb interaction is computed within the Random Phase Approximation (RPA) instead of the plasmon-pole model. Two different ways of computing the self-energy are reported. The method is used successfully to determine the quasiparticle energies of six semiconducting or insulating materials: Si, SiC, AlAs, InAs, NaH and KH. To illustrate the novelty of the method the real and imaginary part of the frequency-dependent self-energy together with the spectral function of silicon are computed. Finally, the GWA results are compared with other calculations, highlighting that all-electron GWA results can differ markedly from those based on pseudopotential approaches.

PACS numbers: 71.15.-m, 71.15.Mb, 71.20.Nr

I. INTRODUCTION

For many weakly correlated materials, the density-functional theory¹(DFT) in the local-density approximation (LDA) provides a good description of their ground-state properties. However, DFT is not able to describe correctly their excited states. Thus, for example, the band gaps in the LDA are typically much smaller than the experimental values. Quasiparticle (QP) electronic-structure calculations beyond the DFT are therefore highly desirable.

The GW approximation (GWA) of Hedin^{2,3}, which produces a good approximation for the electron's self-energy Σ , enables us to make first-principle QP calculations for realistic materials. Thus, the GWA has been successfully applied to the calculation of QP electronic structures of many kinds of materials^{4,5,6,7}. In particular, recent success has been achieved on predicting the metal-insulator transition of bcc hydrogen,⁸ electronic excitations of yttrium trihydride,⁹ as well as the QP electronic structure of copper.¹⁰ Unfortunately, most of the GWA implementations are based on the pseudopotential type of approaches together with plasmon-pole (PIP) models.^{11,12,13,14,15,16} The weakness of these types of calculations is that the imaginary part of the self-energy is not accessible, making it impossible to determine spectral functions and hence to interpret photoemission experiments. In addition the PIP approximation is expected not to hold for systems with localized electrons. Moreover, it has been noticed recently^{15,17} that GWA implementations based on pseudopotential methods lead to larger and more \mathbf{k} -dependent shifts than calculations based on all-electron DFT methods, bringing into ques-

tion the validity of the former approaches.

However, some attempts have been made to go beyond the plasmon-pole approximation.^{7,10,17,18,19,20,21} In particular, Aryasetiawan has approximately determined the screening within the RPA using a linear muffin-tin orbital method within the atomic sphere approximation⁷ (LMTO-ASA). This method, although fast, approximates the space by atomic centered overlapping spheres, thus completely neglecting the interstitial region, and hence making the reliability of the GW method uncertain. Kotani and van Schilfgaarde based their full-potential LMTO GW calculation¹⁷ on the work of Aryasetiawan by taking into account correctly the interstitial region. Nevertheless their method is not quite accurate since in their implementation they didn't take into account the multiplicity of the same angular momenta for a given principal quantum number in the basis set (like simultaneously using the 3d and 4d states). Finally, Ku and Eguluz produced selfconsistent and non-selfconsistent QP band gaps based on an approximate Luttinger-Ward functional,¹⁸ the non-selfconsistent results are much smaller than all existing GW calculations. Since these results are based on a different scheme we have chosen not to discuss their method further. On the other hand, several pseudopotential have produced GW results without resorting to the plasmon-pole approximation. These methods, although interesting, use pseudowave functions and hence can only determine pseudo-matrix elements of operators, making them difficult to justify as quantitative and reliable methods for computing QP properties.

The major purpose of this paper is then to present a new implementation of the GWA method using the all-electron full-potential Projector Augmented-Wave

method (PAW) *complete* basis set, and without using any PIP model for the determination of the dielectric function. The screening of the Coulomb interaction is thus described in the Random Phase Approximation (RPA), avoiding further approximations.

The paper is organized as follows. In section II we describe our implementation of the GW approximation. In Section III we present our QP calculations for Si, SiC, AlAs, and InAs and also for the alkali hydrides compounds NaH and KH (to our knowledge this is the first GWA study of these alkali hydrides). At the end of this section we compare and discuss our results with other calculations and experiments.

II. FORMALISM

A. The PAW method

The PAW formalism has been well-described elsewhere,^{22,23,24,25} so we will not discuss it in this paper. The PAW method²² is a very powerful all-electron method for performing electronic structure calculations within the framework of the LDA. It takes advantage of the simplicity of pseudopotential methods, but describes correctly the nodal behavior in the augmentation regions. The selfconsistent calculation of the electronic structure is performed using the Car-Parinello method over the occupied states. To determine the eigenvalues and eigenvectors of all unoccupied states (up to 200 eV above the top of the valence states) needed for the GW calculations, we have extracted the selfconsistent full-potential, constructed and diagonalized the PAW Hamiltonian for every irreducible \mathbf{k} point in the Brillouin zone.

B. The GW approximation

1. Quasiparticle energies

In general, the QP energies $E_n(\mathbf{k})$ and wave function $\psi_{\mathbf{k}n}(\mathbf{r})$ are determined from the solution of the QP equation

$$\begin{aligned} (T + V_{ext} + V_h)\psi_{\mathbf{k}n}(\mathbf{r}) + \int d^3r' \Sigma(\mathbf{r}, \mathbf{r}', E_n(\mathbf{k}))\psi_{\mathbf{k}n}(\mathbf{r}') \\ = E_n(\mathbf{k})\psi_{\mathbf{k}n}(\mathbf{r}) \end{aligned} \quad (1)$$

where T is the free-electron kinetic energy operator, V_{ext} the external potential due to the ion cores, V_h the average electrostatic (Hartree) potential, and Σ the electron self-energy operator. The major difficulty connected with Eq. (1) is finding an adequate approximation for the self-energy operator $\Sigma(\mathbf{r}, \mathbf{r}', E_n(\mathbf{k}))$. Nonetheless, it was shown by Hedin^{2,3} that writing the self-energy as a product of the Green's function and the screened Coulomb

interaction W yields the successful GW approximation for Σ . In this approximation, both the non-locality and the dynamical correlations are included. Assuming that the difference $\hat{\Sigma} - \hat{V}_{xc}$ between the self-energy and the Kohn-Sham exchange and correlation potential is small, we can use a perturbation theory approach to solve the effective QP Hamiltonian \hat{H}^{qp}

$$\hat{H}^{qp} = \hat{H}_{KS} + (\hat{\Sigma} - \hat{V}_{xc}) \quad (2)$$

and determine the QP energies by expanding the real part of selfenergy to first order around $\epsilon_n(\mathbf{k})$ thus making the comparison with the PIP models possible $\text{Re}E_n(\mathbf{k}) = \epsilon_n(\mathbf{k}) + Z_{n\mathbf{k}} \times$

$$[\langle \Psi_{\mathbf{k}n} | \text{Re}\Sigma(\mathbf{r}, \mathbf{r}', \epsilon_n(\mathbf{k})) | \Psi_{\mathbf{k}n} \rangle - \langle \Psi_{\mathbf{k}n} | V_{xc}^{LDA}(r) | \Psi_{\mathbf{k}n} \rangle] \quad (3)$$

where the QP renormalization factor $Z_{n\mathbf{k}}$ is given by

$$Z_{n\mathbf{k}} = [1 - \langle \Psi_{\mathbf{k}n} | \frac{\partial}{\partial \omega} \text{Re}\Sigma(\mathbf{r}, \mathbf{r}', \epsilon_n(\mathbf{k})) | \Psi_{\mathbf{k}n} \rangle]^{-1}. \quad (4)$$

This assumption is valid for simple *sp* bonded materials, since it was shown that the QP wave function $\psi_{\mathbf{k}n}$ and Kohn-Sham wave function $\Psi_{\mathbf{k}n}$ are almost identical, i.e., the QP Hamiltonian \hat{H}^{qp} is diagonal in the $\Psi_{\mathbf{k}n}$ basis for simple *sp* bonded semiconductors.^{11,12} We therefore assume this behavior for the materials studied in this paper. According to this equation, the LDA eigenvalues $\epsilon_n(\mathbf{k})$ are then corrected by the GW approximation. The numerical work is therefore considerably reduced, but still computationally demanding.

In our implementation, we have calculated the Green's function only for the valence and conduction states. One has then to subtract out only the valence exchange and correlation potential in Eq. (3). To check the accuracy of this procedure, we have also used the so-called Hartree-Fock decoupling,^{15,26} and have found that the average error in the QP energies of Si with respect to the top of the valence states is 0.05 eV. The approximation made here is the one currently used in all pseudopotential-based GWA calculations, making our method compatible with existing GW implementations.

2. Screened Coulomb interaction

For the calculation of the self-energy, one needs to evaluate the dynamically screened interaction $W(\mathbf{r}, \mathbf{r}', \omega)$, which can be rewritten in reciprocal space as:

$$W_{\mathbf{G}, \mathbf{G}'}(\mathbf{q}, \omega) = 4\pi \frac{1}{|\mathbf{q} + \mathbf{G}|} \tilde{\epsilon}_{\mathbf{G}, \mathbf{G}'}^{-1}(\mathbf{q}, \omega) \frac{1}{|\mathbf{q} + \mathbf{G}'|}. \quad (5)$$

The symmetrized dielectric matrix $\tilde{\epsilon}_{\mathbf{G}, \mathbf{G}'}(\mathbf{q}, \omega)$ is defined in the random phase approximation (RPA) by²⁷

$$\begin{aligned} \tilde{\epsilon}_{\mathbf{G}\mathbf{G}'}(\mathbf{q}, \omega) = & \delta_{\mathbf{G}\mathbf{G}'} - \frac{8\pi}{\Omega|\mathbf{q} + \mathbf{G}||\mathbf{q} + \mathbf{G}'|} \sum_{v,c,\mathbf{k}} M_{\mathbf{G}}^{vc}(\mathbf{k}, \mathbf{q}) [M_{\mathbf{G}'}^{vc}(\mathbf{k}, \mathbf{q})]^* \\ & \times \left(\frac{1}{\omega + \epsilon_v(\mathbf{k} - \mathbf{q}) - \epsilon_c(\mathbf{k}) - i\delta} - \frac{1}{\omega - \epsilon_v(\mathbf{k} - \mathbf{q}) + \epsilon_c(\mathbf{k}) + i\delta} \right), \end{aligned} \quad (6)$$

with the following notation:

$$M_{\mathbf{G}}^{nm}(\mathbf{k}, \mathbf{q}) = \langle \Psi_{\mathbf{k}-\mathbf{q}n} | e^{-i(\mathbf{q}+\mathbf{G})\mathbf{r}} | \Psi_{\mathbf{k}m} \rangle, \quad (7)$$

where v and c denote, respectively, the valence and conduction states, and δ a positive infinitesimal. The matrix elements given by Eq. (7) are evaluated using the PAW basis set as described in Ref. 15.

Most of GWA calculations use a kind of PIP approximation. This is computationally efficient since one obtains an analytic expression for the integral in the self-energy. It is not clear, however, that this kind of approximation is valid for describing the QP of different kind of materials. It is for this reason that we have chosen to avoid the PIP model altogether, to compute the dynamical dielectric function in the RPA (6), and to perform the

integral of the selfenergy numerically. In our implementation, we need to compute $\tilde{\epsilon}_{\mathbf{G}\mathbf{G}'}(\mathbf{q}, \omega)$ along the imaginary axis and for some real frequencies. This technical point will become clearer in the next subsection.

To reduce the computational cost of the GWA, we use symmetry properties. Details about the utilization of the symmetry for the static dielectric matrix has been already given elsewhere^{5,15,28,29}, so we just describe briefly how to use the symmetry in the case of the dynamical dielectric function. For the case of pure imaginary frequencies, we could safely ignore the broadening factor $i\delta$; in this case $\tilde{\epsilon}_{\mathbf{G}\mathbf{G}'}(\mathbf{q}, i\omega)$ is hermitian and we could use the symmetry just as in the static case. We can then write the symmetrized dielectric matrix as

$$\begin{aligned} \tilde{\epsilon}_{\mathbf{G}\mathbf{G}'}(\mathbf{q}, i\omega) = & \delta_{\mathbf{G}\mathbf{G}'} - \frac{8\pi}{\Omega|\mathbf{q} + \mathbf{G}||\mathbf{q} + \mathbf{G}'|} \sum_{\mathbf{k} \in BZ_{\mathbf{q}}} \sum_{v,c} \sum_{R \in G_{\mathbf{q}}} M_{R\mathbf{G}}^{vc}(\mathbf{k}, \mathbf{q}) [M_{R\mathbf{G}'}^{vc}(\mathbf{k}, \mathbf{q})]^* \\ & \times \left(\frac{1}{i\omega + \epsilon_v(\mathbf{k} - \mathbf{q}) - \epsilon_c(\mathbf{k})} - \frac{1}{i\omega - \epsilon_v(\mathbf{k} - \mathbf{q}) + \epsilon_c(\mathbf{k})} \right), \end{aligned} \quad (8)$$

where $G_{\mathbf{q}}$ is the little group of the point group G such that $R\mathbf{q} = \mathbf{q}$; R being a symmetry operation. The computational cost is further reduced by noticing that

$$\tilde{\epsilon}_{\mathbf{G}\mathbf{G}'}(R\mathbf{q}, i\omega) = \tilde{\epsilon}_{R^{-1}\mathbf{G}R^{-1}\mathbf{G}'}(\mathbf{q}, i\omega). \quad (9)$$

for real ω , although the dielectric matrix is not hermitian, we could use the symmetry by making a decomposition into hermitian and anti-hermitian parts of the polarizability $P_{\mathbf{G}\mathbf{G}'}(\mathbf{q}, \omega)$. if we define $A_{\mathbf{G}\mathbf{G}'}(\mathbf{q}, \omega)$ and $B_{\mathbf{G}\mathbf{G}'}(\mathbf{q}, \omega)$ by

$$A_{\mathbf{G}\mathbf{G}'}(\mathbf{q}, \omega) = \frac{P_{\mathbf{G}\mathbf{G}'}(\mathbf{q}, \omega) + P_{\mathbf{G}\mathbf{G}'}^\dagger(\mathbf{q}, \omega)}{2} \quad (10)$$

and

$$B_{\mathbf{G}\mathbf{G}'}(\mathbf{q}, \omega) = \frac{P_{\mathbf{G}\mathbf{G}'}(\mathbf{q}, \omega) - P_{\mathbf{G}\mathbf{G}'}^\dagger(\mathbf{q}, \omega)}{2i}, \quad (11)$$

then equations (8) and (9) still hold, allowing us to perform the same computational tasks as for the symmetrized dielectric matrix with imaginary frequencies. This procedure makes it possible to first compute

$W_{\mathbf{G},\mathbf{G}'}(\mathbf{q}, \omega)$ only for irreducible points of the first Brillouin zone (BZ). We then determine easily the screened interaction for all \mathbf{k} -points in the Brillouin zone using symmetry properties.

3. Self Energy

The self energy Σ is the key quantity of any GWA calculation. As previously noticed, we have chosen to avoid plasmon-pole models and compute Σ with the ω dependence of the screened interaction W within the RPA.

First, we split the integral of the selfenergy into a bare exchange or Hartree-Fock contribution Σ^X and an energy dependent contribution $\Sigma^C(\omega)$ which describes self-energy effects beyond Σ^X . The matrix elements of the self-energy are now given by the sum of

$$\langle \Psi_{\mathbf{k}n} | \Sigma^X | \Psi_{\mathbf{k}n} \rangle = -\frac{4\pi}{\Omega} \sum_{\mathbf{q}} \sum_m^{occ} \sum_{\mathbf{G}} \frac{|M_{\mathbf{G}}^{mn}(\mathbf{k}, \mathbf{q})|^2}{|\mathbf{q} + \mathbf{G}|^2} \quad (12)$$

where the summation is over occupied states, and

$$\begin{aligned} & \langle \Psi_{\mathbf{k}n} | \Sigma^C(\omega) | \Psi_{\mathbf{k}n} \rangle \\ &= \frac{1}{\Omega} \sum_{\mathbf{q}} \sum_{\mathbf{G}\mathbf{G}'} \sum_m [M_{\mathbf{G}}^{mn}(\mathbf{k}, \mathbf{q})]^* M_{\mathbf{G}'}^{mn}(\mathbf{k}, \mathbf{q}) \\ & \quad \times C_{\mathbf{G}\mathbf{G}'}^m(\mathbf{k}, \mathbf{q}, \omega) \end{aligned} \quad (13)$$

with

$$\begin{aligned} & C_{\mathbf{G}\mathbf{G}'}^m(\mathbf{k}, \mathbf{q}, \omega) \\ &= \frac{i}{2\pi} \int d\omega' \frac{W_{\mathbf{G}\mathbf{G}'}^C(q, \omega')}{\omega + \omega' - \epsilon_m(\mathbf{k} - \mathbf{q}) + i\delta \text{sgn}(\epsilon_m(\mathbf{k} - \mathbf{q}) - \mu)} \end{aligned} \quad (14)$$

where W^C is defined as $W^C = W - v$, with v being the bare Coulomb potential. To evaluate this integral directly on the real axis one should compute W^C for many points ω' since the shape of W^C along the real axis is rather ragged. Even though this has been done by some authors,¹⁰ we choose to avoid this difficulty by using the fact that W^C is well behaved along the imaginary axis. In the present work, we have performed this integral using two different methods:

In the first one, the contour of the frequency integral (14) is deformed in a way to obtain an integral along the imaginary axis plus contributions from the poles of the Green's function. In this case, we obtain the following expression:

$$\begin{aligned} & C_{\mathbf{G}\mathbf{G}'}^n(\mathbf{k}, \mathbf{q}, \omega) \\ &= -\frac{1}{\pi} \int_0^\infty d\omega'' W_{\mathbf{G}\mathbf{G}'}^C(q, i\omega'') \frac{\omega - \epsilon_n(\mathbf{k} - \mathbf{q})}{(\omega - \epsilon_n(\mathbf{k} - \mathbf{q}))^2 + \omega''^2} \\ & \quad + W_{\mathbf{G}\mathbf{G}'}^C(q, \pm(\omega - \epsilon_n(\mathbf{k} - \mathbf{q}))) \theta(\pm(\omega - \epsilon_n(\mathbf{k} - \mathbf{q}))) \\ & \quad \times \theta(\pm(\omega - \mu)) \theta(\pm(\epsilon_n(\mathbf{k} - \mathbf{q}) - \mu)) \end{aligned}$$

The first term represents the contribution along the imaginary axis and is evaluated by Gaussian quadrature. The second is from the poles of the Green's function and its computation is done by fitting values of W^C at $\pm(\omega - \epsilon_n(\mathbf{k} - \mathbf{q}))$ from values on a given mesh of frequencies⁵⁴. Here μ denotes the Fermi level in the LDA and ω'' is defined to be real. This method is similar to the one used by Aryasetiawan for the implementation of the GWA based on the LMTO method in the atomic sphere approximation⁷ (ASA), and within the GWA of Kotani and coworkers based on the full-potential linear muffin-tin orbital (FP-LMTO) method.¹⁷ The reader can find more details about this integration procedure in Refs. 7,17. Similar work has been also carried out by Bechstedt and coworkers²⁰ as well as by Fleszar and Hanke²¹ starting from a pseudopotential approach.

In our second implementation, which is similar to that of Ref. 19, we evaluate the matrix elements of the correlative part of the self-energy $\langle \Psi_{m\mathbf{k}} | \Sigma^C(\omega) | \Psi_{l\mathbf{k}} \rangle$ for a set of imaginary frequencies $i\omega$, the resulting quantity is then

TABLE I: Calculated quasiparticle energies of silicon for some points in the Brillouin zone with our two different implementations. The results are in good agreement with each other. In the last line, the minimum band gap E_g is presented.

	First method ^a	Second method ^b
Γ_{1v}	-11.85	-11.87
$\Gamma_{25'v}$	0.00	0.00
Γ_{15c}	3.09	3.09
$\Gamma_{2'c}$	4.05	4.06
\mathbf{X}_{1v}	-7.74	-7.68
\mathbf{X}_{4v}	-2.90	-2.91
\mathbf{X}_{1c}	1.01	1.03
\mathbf{X}_{4c}	10.64	10.59
$\mathbf{L}_{2'v}$	-9.57	-9.50
\mathbf{L}_{1v}	-6.97	-6.90
$\mathbf{L}_{3'v}$	-1.16	-1.17
\mathbf{L}_{1c}	2.05	2.03
\mathbf{L}_{3c}	3.83	3.83
E_g	0.92	0.90

^aContour deformation method

^bAnalytic continuation method

analytically continued to the real axis by fitting it to the following Padé form

$$P(z) = \frac{a_0 + a_1 z + a_2 z^2 + \dots + a_N z^N}{b_0 + b_1 z + b_2 z^2 + \dots + b_M z^M} \quad (15)$$

where a_i and b_i are complex parameters that are determined during the fit along the imaginary axis. Values of 5 for N and of 6 for M provided us with an accurate and stable fit. The same kind of continuation has also been applied with success to compute the dynamical response function,^{30,31} so we are confident of its reliability. The main difference between the work presented here and that of Ref. (19) is that our code starts from an all-electron basis, so we are not using fast Fourier transforms to switch between real and reciprocal spaces and between time and frequency domains. Our expression (15) is also different, but we believe that this is of minor importance⁵⁵.

In both cases, the integration over the first Brillouin zone is done by the special-point technique.³² The number of bands as well as the number of \mathbf{G} vectors in (13) is increased until the QP energies are converged. Similarly, the number of frequency points ω' for which W^C is computed is increased until $C_{\mathbf{G}\mathbf{G}'}^n(\mathbf{k}, \mathbf{q}, \omega)$ is well converged. The two different implementations allow us to check carefully our results, and as can be seen in Table I for the case of silicon, the QP energies are insensitive to the method used to compute the self-energy.

4. Treatment of the Coulomb divergence

The last point we wish to discuss is an additional difficulty which occurs when evaluating the self-energy by a summation of the \mathbf{q} points over the full BZ. We cannot apply the special-point technique directly since the integrands have a $1/\mathbf{q}^2$ singularity for $\mathbf{q} \rightarrow 0$ as can be seen for example by putting $\mathbf{G} = 0$ in the expression of the exchange term given by (12). The difficulty can be removed by adding and subtracting a term which has the same singularities as the initial expression, and which can be evaluated numerically and analytically. As a consequence, the integrals over the BZ are rewritten

$$\sum_{\mathbf{q}} G(\mathbf{q}) = \sum_{\mathbf{q}} [G(\mathbf{q}) - A F(\mathbf{q})] + A \sum_{\mathbf{q}} F(\mathbf{q}), \quad (16)$$

where $F(q)$ is an auxiliary periodic function that diverges like $1/\mathbf{q}^2$ as \mathbf{q} vanishes. The term is regular and can be evaluated by the special point technique whereas the last sum is evaluated analytically. For the exchange term, it is not difficult to evaluate A in (16), but it gets more complicated for the correlative part of the self-energy (13). The purpose of the offsetted Γ -point method¹⁷ is to avoid the evaluation of the quantity A , but still to be able to deal with the divergence. The main idea is to find a new mesh of points such that

$$\sum_{\mathbf{q}} F(\mathbf{q}) = \sum_{\mathbf{q}'} F(\mathbf{q}') \quad (17)$$

where the Γ -point is included in the old mesh \mathbf{q} but not in the new one \mathbf{q}' : the Γ -point is replaced by other points (different from Γ) to construct the \mathbf{q}' grid in order to fulfill Eq. (17). Eq. (16) is therefore rewritten as:

$$\sum_{\mathbf{q}} G(\mathbf{q}) = \sum_{\mathbf{q}} [G(\mathbf{q}) - A F(\mathbf{q})] + A \sum_{\mathbf{q}'} F(\mathbf{q}'), \quad (18)$$

Then we show by inspection that the term $\sum_{\mathbf{q}} [G(\mathbf{q}) - A F(\mathbf{q})]$ is equal to $\sum_{\mathbf{q}'} [G(\mathbf{q}') - A F(\mathbf{q}')] + A \sum_{\mathbf{q}'} F(\mathbf{q}')$ with a controlled error, Eq. (18) transforms to

$$\sum_{\mathbf{q}} G(\mathbf{q}) = \sum_{\mathbf{q}'} G(\mathbf{q}') \quad (19)$$

because the two terms which contain the function $F(\mathbf{q})$ cancel out since they are evaluated on the same \mathbf{q}' grid. We have therefore avoided the evaluation of the complicated A term in Eq. (16).

The remaining points to be addressed are the choice of the function $F(\mathbf{q})$ and the number of additional points for the new mesh used to solve (17). In our case, we write

$$F(\mathbf{q}) = \sum_{\mathbf{G}} \frac{\exp(-|\mathbf{q} + \mathbf{G}|^2)}{|\mathbf{q} + \mathbf{G}|^2}$$

and choose to add 6 points to the original \mathbf{q} mesh in order to get the new mesh. Equation (17) is then solved

TABLE II: Lattice constants a (in atomic units) and energy cut offs E_{cut} (in Rydberg) used for our PAW calculations. The lattice constants are from Ref. 35, unless stated otherwise.

	a	E_{cut}
Si	10.26	20
SiC	8.24	25
AlAs	10.67	20
InAs	11.41	20
NaH	9.28 ^a	40
KH	10.83 ^a	40

^aReference 36

to provide us with the coordinates of the new 6 points in the BZ.⁵⁶ The computational cost is further reduced by finding equivalent points among those 6 points, and we end up with well behaved and easily evaluated BZ sums.

III. NUMERICAL RESULTS AND DISCUSSION

In this section we present our theoretical quasiparticle energies for the six materials studied in this paper, together with the available theoretical and experimental results. In Sec. III A we report our results for four semiconductors (Si, SiC, AlAs, InAs) of zinc-blende type structure, while Sec. III B is devoted to studying the alkali hydrides NaH and KH in the rocksalt phase. Table II presents the experimental lattice parameters and the energy cut offs E_{cut} used for the final converged calculations.

A. Results for Si, SiC, AlAs, and InAs

Silicon is probably the most carefully studied semiconductor, and several GWA results are available. Using silicon as a prototype will allow us to test our method by making careful comparisons with previous GWA calculations. As mentioned earlier, our code presents two different ways for calculating the self-energy. We therefore test their accuracy for silicon in Table I. We find that the results of the two methods are almost identical, showing that they are equally reliable for computing the self-energy. In particular, our implementation with the extrapolation procedure makes it possible to represent the full-frequency dependence of the self-energy with a small additional computational cost. Fig. 1 shows the real and imaginary parts of Σ along the real axis for silicon at the Γ point for a wide range of frequencies. The agreement with previous work is excellent.¹⁹

A special feature of our work is the possibility of obtaining the imaginary part of the self-energy (see Fig. 1), a task virtually impossible within the PIP approximation⁵⁷. The spectral function which can be obtained directly from the self-energy

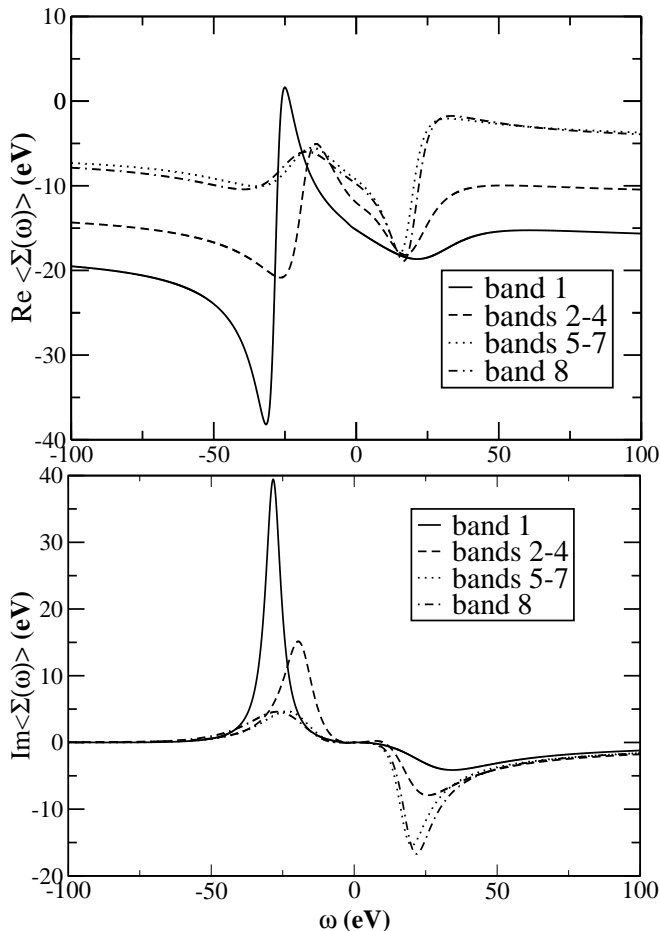


FIG. 1: $\text{Re}\langle\Psi_{\mathbf{k}m}|\Sigma(\omega)|\Psi_{\mathbf{k}m}\rangle$ and $\text{Im}\langle\Psi_{\mathbf{k}m}|\Sigma(\omega)|\Psi_{\mathbf{k}m}\rangle$ shown for the first 8 bands for silicon at $\mathbf{k} = \mathbf{0}$. The zero of energy is at the center of the band gap.

$$\langle\Psi_{\mathbf{k}m}|A(\omega)|\Psi_{\mathbf{k}m}\rangle =$$

$$\frac{|\text{Im}\langle\Psi_{\mathbf{k}m}|\Sigma(\omega)|\Psi_{\mathbf{k}m}\rangle|}{[\omega - \epsilon_m(\mathbf{k}) - \text{Re}\langle\Psi_{\mathbf{k}m}|\Sigma(\omega)|\Psi_{\mathbf{k}m}\rangle]^2 + [\text{Im}\langle\Psi_{\mathbf{k}m}|\Sigma(\omega)|\Psi_{\mathbf{k}m}\rangle]^2}$$

is of major interest since it can be used for the interpretation of experimental photoemission and inverse-photoemission spectra. As an example, the spectral function of silicon at the Γ point is shown in Fig. 2. The sharp peaks correspond to QP excitations, while the incoherent part of the function, the spectral background, is much complicated and could correspond to plasmon type excitations.

The QP calculations have been performed using 256 \mathbf{k} points in the full BZ. The size of the dielectric matrix defined in Eq. (6) is 137×137 for silicon and SiC, 169×169 for AlAs, 181×181 for InAs. 200 bands were used for the sum over conduction states in Eq. (6) and for the sum over m in Eq. (13). Due to the smoothness of the integrand along the imaginary axis, 11 points are found sufficient to obtain well converged quantities. An energy step of 1.5 eV is used for the part of Eq. (15) which corresponds to the poles of the Green's function. Using

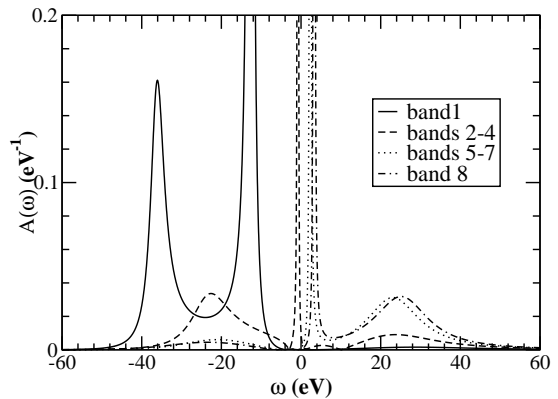


FIG. 2: Spectral function $\langle\Psi_{\mathbf{k}m}|A(\omega)|\Psi_{\mathbf{k}m}\rangle$ for the first 8 bands for silicon at $\mathbf{k} = \mathbf{0}$. The zero of energy is at the center of the band gap. The sharp peaks are QP poles, their weights correspond to the factor Z defined in Eq. 4.

this energy step we determine an energy grid which we use to produce an accurate fit to $W_{\mathbf{G}\mathbf{G}'}^C(q, \pm(\omega - \epsilon_n(\mathbf{k} - \mathbf{q})))$ for the different points $\pm(\omega - \epsilon_n(\mathbf{k} - \mathbf{q}))$. All these high values of the parameters ensure the convergence of the QP energies to within 0.05 eV.

Table III shows the excellent agreement of our results with two other all-electron GWA implementations of the QP energies of silicon. From this table it seems that, at least for Si, the overall difference between the RPA and the PIP results is small.⁵⁸ Nevertheless, a discrepancy of as much as 0.18 eV for the energy of \mathbf{L}_{1v} is obtained. It seems then, at least for Si, the PIP model overestimates only slightly the differences between the energy levels within the GWA.

Table IV compares the calculated QP energies for 3C-SiC (also known as β -SiC), AlAs and InAs with experimental data as well as with pseudopotential-GWA (PP-GWA) calculations. The band gaps are given at Γ , X , and L and are underlined in this table. These studies are motivated by the fact that SiC is a material of high current technological interest and that InAs is predicted to be metallic in the LDA, whereas AlAs is used as a test case. A general trend of our implementation is that the agreement with experiment as well as with PP-GWA results is not perfect, as also found by other implementations based on all-electron methods;^{15,17} reporting differences up to 0.4 eV. In particular, the largest difference occurs for the $\Gamma_{25v}^* \rightarrow \mathbf{X}_{1c}$ transition.⁵⁹ We showed in a previous study¹⁵ for the case of silicon that these differences are mainly traced back to differences between the exchange-correlation matrix elements obtained by the two methods. We believe that this can be extended to other materials as well, since it seems to be a general feature⁶⁰ of all-electron GWA calculations.

In fact, the difference between all-electron and PP based GW calculations is not surprising since the use of pseudo-wave functions for evaluating matrix elements of a general operator produce results that may not be sufficiently precise, because the pseudo-wave functions

TABLE III: Selected energy eigenvalues, in eV, at Γ , X and L for Si. Our results are compared with two other all-electron implementations of the GW method and with experimental results. Data in parentheses are results when the denominator of the Green's function is updated with QP energies. Data in the last line correspond to the minimum energy gap E_g .

	LDA		GW approximation			Expt. ^c
	Present	LAPW ^a	Present	PAW-PIP ^b	LAPW ^a	
Γ_{1v}	-11.97	-11.95	-11.85 (-11.89)	-11.92	-12.21	-12.5±0.6
Γ'_{25v}	0.00	0.00	0.00 (0.00)	0.00	0.00	0.00
Γ_{15c}	2.54	2.55	3.09 (3.15)	3.16	3.30	3.40, 3.05 ^d
Γ'_{2c}	3.23	3.17	4.05 (4.12)	4.09	4.19	4.23, 4.1 ^d
X_{1v}	-7.82	-7.82	-7.74 (-7.78)	-7.91	-8.11	
X_{4v}	-2.85	-2.84	-2.90 (-2.92)	-2.98	-3.03	-2.9 ^e , -3.3±0.2 ^f
X_{1c}	0.61	0.65	1.01 (1.08)	1.10	1.14	1.25 ^d
X_{4c}	10.02		10.64 (10.72)	10.74		
L'_{2v}	-9.63	-9.63	-9.57 (-9.60)	-9.66	-9.92	-9.3±0.4
L_{1v}	-6.99	-6.98	-6.97 (-7.00)	-7.15	-7.31	-6.7±0.2
L'_{3v}	-1.19	-1.19	-1.16 (-1.17)	-1.24	-1.26	-1.2±0.2
L_{1c}	1.44	1.43	2.05 (2.11)	2.08	2.15	2.1 ^g , 2.4±0.15
L_{3c}	3.30	3.35	3.83 (3.90)	3.92	4.08	4.15±0.1 ^h
E_g	0.55	0.52	0.92 (0.95)	0.97	1.01	1.17

^aReference 14

^bReference 15

^cUnless noted, Ref 35

^dReference 38

^eReference 39

^fReference 40

^gReference 41

^hReference 42

are constructed to reproduce the all-electron wave functions only in the interstitial region, i.e., outside the atomic spheres. This is however a good representation for studying properties that depend only on the behavior of the wave function in the bonding region. An error is then introduced in any PP-GWA calculation. This error seems to fortuitously have a tendency to improve the agreement with experiment, explaining the exceptional success of the PP-GWA.

For InAs, the incorrect metallic behavior obtained within the LDA is corrected by our GWA calculation. The GWA produces the true semiconducting state as given by experiment. Since we did not account for the spin-orbit coupling in our calculation, we have simply averaged out the spin-orbit-split experimental values to make the comparison with our work possible.

B. Results for the alkali hydrides NaH and KH

Alkali hydride materials exhibit a structural phase transition from the B1 (NaCl structure) to the B2 (CsCl structure) type structure under hydrostatic pressure. A number of studies have been performed to understand the equation of state of these materials,^{36,37,48,49} as well as the possibility of an insulator-metal transition,^{50,51} how-

ever only few studies have been published about the electronic structures.^{48,49,52} In these materials, hydrogen behaves as an H^- ion, leading to partly ionic materials with a larger band gap than the studied ' sp ' semiconductors. It is, therefore, of interest to know whether the GWA is capable of producing such large band gaps. In this study we are only concerned with the determination of their QP energies for the rocksalt crystallographic structure.

In Fig. 3 we report the QP band structures of NaH and KH along some high-symmetry directions,⁶¹ and present a detailed overview of their LDA and QP energies in Table V. In the following we detail and compare our results with existing experimental and calculated results: For NaH, the authors of Ref. 48 reported an LDA calculation with an improved LMTO method in its atomic sphere approximation, however, from their band structure plot we estimated that their band gap is only about 2.7 eV and is direct at the L point. This disagrees with our calculation, since at the LDA level we found an indirect band gap of 3.39 eV from W to L . This could be due to Ref. 48's use of a different value of the lattice parameter of 8.90 a.u. A calculation by Kunz and Michish⁴⁹ based on the electronic polaron model produced a direct band gap at X of 1.52 eV, a value too low for these ionic materials, so that it should be taken only at a qualitative level.⁶² However, our LDA results are in full agreement with results of Ref. 52, where an indirect band gap from

TABLE IV: Quasiparticle energies in eV at Γ , X and L for SiC, AlAs, and InAs. Data in parentheses are results when the denominator of the Green's function is updated with QP energies. Our results are compared with PP-GW method and with experimental results (minimum band gaps are underlined).

	LDA		GW		Expt ^a
	Present	PP ^b	Present	PP ^b	
SiC					
$\Gamma'_{25v} \rightarrow \Gamma_{15c}$	6.25	6.41	7.32(7.45)	7.35	
$\Gamma'_{25v} \rightarrow \mathbf{X}_{1c}$	<u>1.28</u>	<u>1.31</u>	<u>1.80(1.89)</u>	<u>2.34</u>	<u>2.39</u>
$\Gamma'_{25v} \rightarrow \mathbf{L}_{1c}$	5.34	5.46	<u>6.45(6.56)</u>	6.53	4.2
AlAs					
$\Gamma'_{25v} \rightarrow \Gamma_{15c}$	1.94	1.77	2.72(2.79)	2.75	3.11 ^c
$\Gamma'_{25v} \rightarrow \mathbf{X}_{1c}$	<u>1.32</u>	<u>1.20</u>	<u>1.57(1.65)</u>	<u>2.08</u>	<u>2.24</u>
$\Gamma'_{25v} \rightarrow \mathbf{L}_{1c}$	2.06	1.89	2.73(2.80)	2.79	2.49 ^c ;2.54 ^d
InAs					
$\Gamma'_{25v} \rightarrow \Gamma_{15c}$	<u>-0.07</u>	<u>-0.39</u>	0.46(0.49)	<u>0.59</u>	<u>0.60</u>
$\Gamma'_{25v} \rightarrow \mathbf{X}_{1c}$	1.48		1.57 (1.61)	2.10	
$\Gamma'_{25v} \rightarrow \mathbf{L}_{1c}$	1.05		1.54 (1.58)	1.52	1.74

^aUnless noted Ref 35. For InAs, data have been averaged to account for the neglect of spin-orbit coupling in our case.

^bFor SiC, PP results are from Ref. 43, for AlAs from Ref. 44, for InAs from Ref. 45 and averaged to account for the neglect of spin-orbit splitting.

^cReference 46.

^dReference 47.

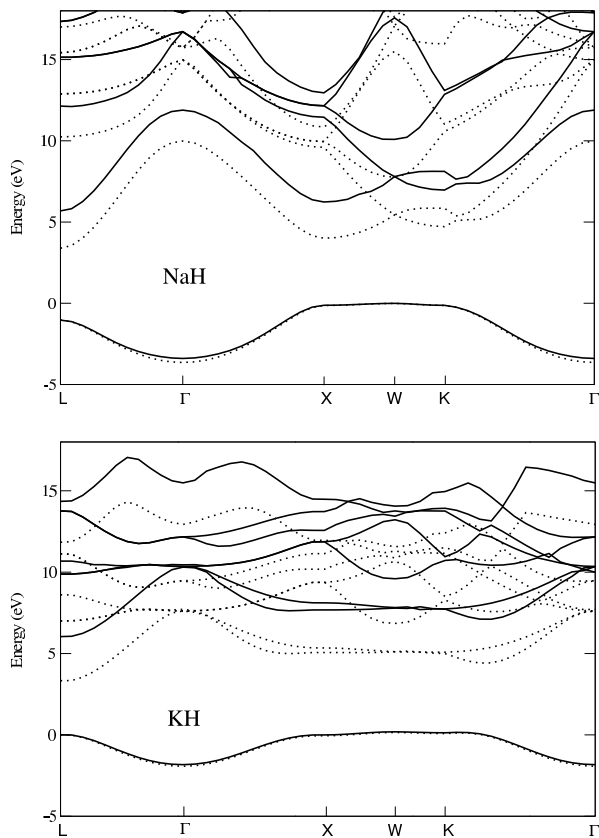


FIG. 3: Calculated LDA (dotted lines) and GW (full lines) electronic band structures of NaH and KH along some high-symmetry directions. These calculations are performed using the parameters reported in Table II.

W to L of about 3.3 eV was found. Table V shows that the energy level differences of NaH are substantially increased by the use of the GWA compared with the LDA results. In particular, the minimum band gap is 5.68 eV within the GWA, whereas it's only 3.39 eV within the LDA. An other interesting point is that we found that the most used scissors-operator shift seems not to apply for the computation of optical properties of NaH. This is because the band gap is increased by 1.66 eV at the Γ point, and as much as 2.34 eV for the direct transition at L point. A GWA calculation of the QP energies in the full BZ is then required for the study the optical properties of NaH. Table V shows also our LDA and QP results for potassium hydride. Our LDA results are in good agreement with the calculation in Ref. 52. We find that in both LDA and GWA calculations, the band gap is indirect from W to L , and could easily switch to a direct gap with a small lattice parameter variation since the valence band (1s state of hydrogen) is very flat, i.e., the valences states at the X , L , W , and K have the same energies within 0.2 eV accuracy. The previous remark about the non-validity of the scissors-operator shift still holds here for the same reasons. The LDA band gap increases by an amount of 2.29 eV at Γ , and as much as

TABLE V: Quasiparticle energies in eV at Γ , X , L , W , and K for NaH and KH. The last line shows the minimum band gap E_g . Data in parentheses are results when the denominator of the Green's function is updated with QP energies. We are not aware of any experimental study concerning the electronic band structure of these materials.

	NaH			KH		
	LDA	GW	(QP)	LDA	GW	(QP)
Γ_{1v}	-3.64	-3.39	(-3.59)	-2.07	-2.02	(-2.11)
Γ_{1c}	9.98	11.89	(12.38)	7.47	9.81	(10.43)
$\Gamma_{25'c}$	14.98	16.71	(17.24)	7.57	10.16	(10.74)
Γ_{15c}	15.72	17.87	(18.11)	9.33	11.98	(12.53)
X_{1v}	-0.13	-0.12	(-0.12)	-0.18	-0.18	(-0.20)
$X_{4'c}$	4.00	6.23	(6.66)	4.91	7.49	(8.01)
X_{3c}	9.59	11.45	(11.96)	5.18	7.92	(8.47)
$X_{5'c}$	9.95	12.15	(12.60)	8.76	11.68	(12.24)
X_{1c}	10.84	12.95	(13.36)	9.27	12.31	(12.86)
L_{1v}	-1.03	-1.03	(-1.06)	-0.15	-0.19	(-0.20)
$L_{2'c}$	3.39	5.68	(6.11)	3.18	5.85	(6.35)
L_{1c}	10.24	12.13	(12.59)	6.86	9.69	(10.23)
$L_{3'c}$	12.89	15.14	(15.61)	8.46	10.49	(11.18)
L_{3c}	15.42	17.34	(17.77)	10.98	13.57	(14.03)
W_{1v}	0.00	0.00	(0.00)	0.00	0.00	(0.00)
W_{3c}	5.43	7.79	(8.24)	4.96	7.60	(8.13)
$W_{2'c}$	7.75	10.08	(10.55)	6.70	9.40	(9.94)
W_{1c}	15.50	17.57	(17.98)	10.50	13.03	(13.55)
W_{3c}	17.08	19.16	(19.57)	10.73	13.25	(13.78)
K_{1v}	-0.13	-0.12	(-0.12)	-0.06	-0.06	(-0.07)
K_{3c}	4.71	6.96	(7.41)	4.84	7.50	(8.02)
K_{1c}	5.84	8.11	(8.56)	4.94	7.62	(8.18)
K_{4c}	10.57	12.85	(13.27)	8.13	10.72	(11.38)
K_{1c}	11.02	13.09	(13.52)	8.36	10.94	(11.54)
E_g	3.39	5.68	(6.11)	3.18	5.85	(6.35)

2.71 eV at the L point.

It is surprising to notice that, across the whole Brillouin zone, the GW band gap shift of KH is larger than that of NaH despite that the LDA band gap of NaH is larger than that of KH. The reason for this puzzling large shift is that the screening of the Coulomb potential in KH is found to be less efficient than in NaH. Indeed, we have found that the RPA static dielectric function of NaH is 3.43 much larger than that of KH which is about 2.62. The hybridization is also less strong for KH than for NaH, since the band width of hydrogen s -states is about 2.02 eV for KH (much smaller than the 3.64 eV band width of NaH). As a consequence, the higher excited states are lower in energy, across the Brillouin zone, by about 2 to 5 eV for KH than for NaH. We hope that our predictive results will stimulate experimentalists to perform photoemission or optical studies of these interesting materials.

IV. CONCLUSION

We have presented an implementation of the GWA using the all-electron PAW method where the screened Coulomb interaction is obtained using the RPA dynamical dielectric function. Thus we avoided the use of the plasmon-pole approximation. We have applied it to study the QP energies of Si, SiC, AlAs, and InAs and found that a precise comparison with other available theoretical and experimental results shows that sometimes the GWA can lead to noticeable discrepancies with experiments. Those discrepancies are generally not so pronounced in the pseudopotential GWA calculations using PIP models. We argued that the approximations used in the pseudopotential method have a tendency to fortuitously improve the agreement with experiment.

We have presented detailed results for the first time for NaH and KH alkali hydrides, and showed that the GWA enhanced substantially the LDA band gaps, motivating further theoretical and experimental studies.

Since our method can compute the imaginary part of the self-energy, we could then determine the QP lifetimes, a task not possible using the PIP approximation. Further inspection of spectral properties as well

as the computation of QP lifetimes will be presented in future work. The method is currently being applied to determine the excitation properties of LiH, and the results will be reported elsewhere.⁵³ Moreover, the use of symmetry and an efficient implementation make us confident that we will soon be able to study systems with a large number of atoms per unit cell, like surfaces or polymers. Furthermore, because we use a mixed basis-set in our implementation we could study systems with localized 'd' or 'f' electrons with a reduced computational cost compared with methods based only a plane wave basis-set.

Acknowledgments

One of us (S. L.) is particularly grateful to W. E. Pickett since part of this work was done during a visit to the University of California Davis supported by DOE grant DE-FG03-01ER45876. Supercomputer time was provided by CINES (project gem1100) on the IBM SP3. This research was supported in part by the National Science Foundation under Grant No. PHY99-07949.

-
- ¹ P. Hohenberg and W. Kohn, Phys. Rev. **136** (1964); W. Kohn and L.J Sham, Phys. Rev. **140**, A1113 (1965).
² L. Hedin, Phys. Rev. **139**, A796 (1965).
³ L. Hedin and S. Lundquist, in *Solid State Physics*, edited by H. Ehrenreich, F. Seitz, and D. Turnbull (Academic, New York, 1969), Vol. 23, p. 1.
⁴ F. Aryasetiawan and O. Gunnarsson, Rep. Prog. Phys. **61**, 237-312 (1998).
⁵ W. G. Aulbur, L. Jönsson, and J. W. Wilkins, 'Quasiparticle calculations in solids', in *Solid State Physics*, edited by H. Ehrenreich and F. Spaegen, vol **54**.
⁶ G. Onida, L. Reining, and A. Rubio, Rev. Mod. Phys. **74**, 601 (2002).
⁷ F. Aryasetiawan, "Advances in Condensed Matter Science," edited by I. V. Anisimov (Gordon and Breach 2000).
⁸ J.-L. Li, G.-M. Rignanese, E. K. Chang, X. Blase, and S. G. Louie, Phys. Rev. B **66**, 035102 (2002).
⁹ P. van Gelderen, P. A. Bobbert, P. J. Kelly, G. Brocks, and R. Tolboom, Phys. Rev. B **66**, 075104 (2002).
¹⁰ A. Marini, G. Onida, and R. Del Sole, Phys. Rev. Lett. **88**, 016403 (2002).
¹¹ M. S. Hybertsen and S. G. Louie, Phys. Rev. B **34**, 5390 (1986).
¹² R. W. Godby, M. Schluter, and L. J. Sham, Phys. Rev. B **37**, 10159 (1988).
¹³ M. Rohlfing, P. Krüger and J. Pollmann, Phys. Rev. B **57**, 6485 (1998).
¹⁴ N. Hamada, M. Hwang and A.J. Freeman, Phys. Rev. B **41**, 3620 (1990).
¹⁵ B. Arnaud and M. Alouani Phys. Rev. B **62**, 4464 (2000).
¹⁶ J. Furthmüller, G. Cappellini, H.-Ch. Weissker, and F. Bechstedt, Phys. Rev. B **66**, 045110 (2002).
¹⁷ T. Kotani and M. Van Schilfgaarde, Solid State Comm. **121**, Issues 9-10, 461 (2002).
¹⁸ W. Ku and A. G. Eguiluz, Phys. Rev. Lett **89**, 12401 (2002).
¹⁹ H. N. Rojas, R. W. Godby, and R. J. Needs, Phys. Rev. Lett **74**, 1827 (1995).
²⁰ F. Bechstedt, M. Fiedler, C. Kress, R. Del Sole Phys. Rev. B **49**, 7357 (1994).
²¹ A. Fleszar and W. Hanke Phys. Rev. B **56**, 10228 (1997).
²² P.E Blöchl, Phys. Rev. B **50**, 17953 (1994).
²³ G. Kresse and D. Joubert, Phys. Rev. B. **59**, 1758 (1999).
²⁴ N. A. W. Holzwarth, G. E. Matthews, R. B. Dunning, A. R. Tackett, and Y. Zeng, Phys. Rev. B **55**, 2005 (1997).
²⁵ N. A. W. Holzwarth, G. E. Matthews, A. R. Tackett, and R. B. Dunning, Phys. Rev. B **57**, 11827 (1998).
²⁶ S. Massidda, M. Posternak, and A. Baldereschi, Phys. Rev. B **48**, 5058 (1993).
²⁷ S. D. Adler, Phys. Rev. **126**, 413 (1962); N. Wisser, Phys. Rev. **129**, 62 (1963), see also D. L. Johnson, Phys. Rev. B **9**, 4475 (1974).
²⁸ M. S. Hybertsen and S. G. Louie, Phys. Rev. B **34**, 5390 (1986).
²⁹ W. G. Aulbur, PhD thesis, The Ohio State University, 1996.
³⁰ Y.-G. Jin and K. J. Chang, Phys. Rev. B **59**, 14841 (1999).
³¹ K.-H. Lee and K. J. Chang, Phys. Rev. B **54**, 8285 (1996).
³² H. J. Monkhorst and J.D. Pack, Phys. Rev. B **13**, 5188 (1976).
³³ F. Gygi and A. Baldereschi, Phys. Rev. B **34**, 4405 (1986).
³⁴ B. Wenzien, G. Cappellini, and F. Bechstedt, Phys. Rev. B **51**, 14701 (1995).
³⁵ *Numerical Data and Functional Relationships in Science and Technology*, edited by K.H. Hellwege and O. Madelung, Landolt-Börnstein, New Series, Group **III**,

- Vols. 17a and 22a (Springer, Berlin, 1982).
- ³⁶ J. L. Martins, Phys. Rev. B **41**, 7883 (1990).
- ³⁷ R. Ahuja, O. Eriksson, and B. Johansson, Physica B **265**, 87 (1999).
- ³⁸ J. E. Ortega and F.J. Himpsel, Phys. Rev. B **47**, 2130 (1993).
- ³⁹ W. E. Spicer and R. C. Eden, in *Proceedings of the Ninth International Conference on the Physics of Semiconductors*, Moscow, 1968, edited by S. M. Ryvkin (Nauka, Leningrad, 1968), Vol. 1, p. 61.
- ⁴⁰ A. L. Wachs, T. Miller, T. C. Hsieh, A.P. Shapiro, and T.C. Chiang, Phys. Rev. B **32**, 2326 (1985).
- ⁴¹ R. Hulthén and N. G. Nilsson, Solid State Comm. **18**, 1341 (1976).
- ⁴² F. J. Himpsel, P. Heimann, and D. E. Eastman, Phys. Rev. B **24**, 2003 (1981).
- ⁴³ M. Rohlfing, P. Krüger and J. Pollmann, Phys. Rev. B **48**, 17791 (1993).
- ⁴⁴ E. L. Shirley, X. Zhu and S. G. Louie, Phys. Rev. B **56**, 6648 (1997).
- ⁴⁵ X. Zhu and S. G. Louie, Phys. Rev. B **43**, 14142 (1991).
- ⁴⁶ D. J. Wolford and J.A. Bradley, Solid State Comm. **53**, 1069 (1985).
- ⁴⁷ D.E. Aspnes and A. A. Studna, Phys. Rev. B **27**, 985 (1983); D. E. Aspnes, S. M. Kelso, R.A. Logan, and R. Bhatt, J. Appl. Phys. **60**, 754 (1986).
- ⁴⁸ C. O. Rodriguez and M. Methfessel, Phys. Rev. B **45**, 90 (1992).
- ⁴⁹ A. B. Kunz and D. J. Mickish, Phys. Rev. B **11**, 1700 (1975).
- ⁵⁰ J. Hama and N. Kawakami, Phys. Lett. A **126**, 348 (1988).
- ⁵¹ N. I. Kulikov, Fiz. Tverd. Tela (Leningrad) **20**, 2027 (1978).
- ⁵² Database compiled by D. A. Papaconstantopoulos and coworkers and located at <http://manybody.nrl.navy.mil/esdata/database.html>
The calculations were performed by the APW method including scalar-relativistic corrections within the LDA.
- ⁵³ S. Lebègue, B. Arnaud, M. Alouani, and W. E. Pickett, to be published.
- ⁵⁴ We have used a simple four point interpolation method. The use of a more elaborate method like the cubic spline method is shown to not influence the final results.
- ⁵⁵ The reason for not using the same expression as in Ref. 19 is that our expression (15) is more general and provided us with a better stability in the fitting procedure.
- ⁵⁶ To justify the use of the present expression for $F(\mathbf{q})$, we have also used the function given by Ref. 33 and found that the final QP energies differ by at most 0.02 eV for silicon. Moreover, the $F(\mathbf{q})$ is specific to fcc lattice systems and therefore must be adapted for other systems according to Ref. 34, whereas the function used in this work is independent of crystallographic system. We have also checked if 6 points are sufficient by performing calculations using a set of 12 points, the resulting QP energies remain unchanged, proving the validity of our choice.
- ⁵⁷ The imaginary part of the self-energy is a sum of delta functions in the plasmon-pole approximation.
- ⁵⁸ Notice that the same PAW method is used to compute the Si QP energies both within the RPA and the PIP model.
- ⁵⁹ Inspection of results of Table IV shows that the $\Gamma'_{25v} \rightarrow \mathbf{L}_{1c}$ for SiC seems to be largely overestimated by GW calculations. In fact, we join the conclusion of Ref. 43 and claim that the experimental value is certainly less precise. This is confirmed by the fact that our calculation agrees by about 0.08 eV with their data.
- ⁶⁰ Using the second method presented in this paper (i. e., the analytic continuation method) did not change the value of the $\Gamma'_{25v} \rightarrow \mathbf{X}_{1c}$ transition by more than 0.05 eV.
- ⁶¹ For the calculated electronic properties of NaH and KH alkali hydrides we have used 64 \mathbf{k} -points in the full BZ as well as 200 bands, and a dielectric matrix of size 169×169 to achieve well converged results.
- ⁶² Kunz and Mickish have also reported a band gap for LiH of 6.61 eV compared to a measured value of 4.99 eV (data reported in the paper of S. Baroni *et al.*, Phys. Rev. B **32**, 4077 (1985)).